PNAS RESEARCH ARTICLE | IMMUNOLOGY AND INFLAMMATION

Structural basis for EROS binding to human phagocyte NADPH oxidase NOX2

Shiyu Liang[a,1], Aijun Liu[a,b,1], Yezhou Liu[a,c], Fuxing Wang[a], Youli Zhou[a], Yuanzhengyang Long[a], Tao Wang[c,d], Zheng Liu[a], Ruobing Ren[e], and Richard D. Ye[a,f,2]

Edited by Stephen Harrison, Boston Children's Hospital, Boston, MA; received November 20, 2023; accepted April 11, 2024

Essential for reactive oxygen species (EROS) protein is a recently identified molecular chaperone of NOX2 (gp91^{phox}), the catalytic subunit of phagocyte NADPH oxidase. Deficiency in EROS is a recently identified cause for chronic granulomatous disease, a genetic disorder with recurrent bacterial and fungal infections. Here, we report a cryo-EM structure of the EROS–NOX2–p22^{phox} heterotrimeric complex at an overall resolution of 3.56Å. EROS and p22^{phox} are situated on the opposite sides of NOX2, and there is no direct contact between them. EROS associates with NOX2 through two antiparallel transmembrane (TM) α-helices and multiple β-strands that form hydrogen bonds with the cytoplasmic domain of NOX2. EROS binding induces a 79° upward bend of TM2 and a 48° backward rotation of the lower part of TM6 in NOX2, resulting in an increase in the distance between the two hemes and a shift of the binding site for flavin adenine dinucleotide (FAD). These conformational changes are expected to compromise superoxide production by NOX2, suggesting that the EROS-bound NOX2 is in a protected state against activation. Phorbol myristate acetate, an activator of NOX2 in vitro, is able to induce dissociation of NOX2 from EROS with concurrent increase in FAD binding and superoxide production in a transfected COS-7 model. In differentiated neutrophil-like HL-60, the majority of NOX2 on the cell surface is dissociated with EROS. Further studies are required to delineate how EROS dissociates from NOX2 during its transport to cell surface, which may be a potential mechanism for regulation of NOX2 activation.

NADPH oxidase | NOX2 | EROS | neutrophils | chronic granulomatous disease

Significance

Essential for reactive oxygen species (EROS) is a recently identified molecular chaperone of NOX2, but the structural basis and functional impact of EROS–NOX2 interaction remains unclear. We present a high-resolution cryo-electron microscopy structure of EROS bound to the NOX2–p22^{phox} complex. EROS and p22^{phox} are situated on opposite sides of NOX2 without direct contact. EROS interaction with NOX2 causes bending of its transmembrane helices TM2 and TM6 that partially blocks the cytoplasmic DH domain for access by FAD and NADPH, thereby compromising electron transfer through NOX2. These findings suggest a potential mechanism for EROS protection of NOX2 against proteolytic degradation and spontaneous activation.

Chronic granulomatous disease (CGD) is a genetic disorder characterized by frequent and sometimes life-threatening bacterial and fungal infections (1). Children with CGD are often healthy at birth, but develop symptoms of severe infections in infancy and early childhood (2). Phagocytes isolated from CGD patients are found defective in bactericidal functions but normal in phagocytosis, leading to the formation of granulomas that isolate the engulfed bacteria and fungi (3, 4). Genetic studies of CGD patients led to the finding of mutations in the NADPH oxidase that is composed of the integral membrane proteins gp91^{phox} (NOX2) and p22^{phox}, the cytosolic factors p67^{phox}, p47^{phox}, p40^{phox}, and the small GTPase Rac (5, 6). In resting phagocytes, NOX2 is inactive and the cytosolic factors are separate from the membrane components. The activation of NADPH oxidase requires translocation of the cytosolic factors to plasma or phagosome membrane and assembly of an active complex for one-electron reduction of molecular oxygen and superoxide production by the catalytic subunit NOX2 (6–8). In phagosomes, superoxide is rapidly converted to other reactive oxygen species (ROS) such as hydrogen peroxide (H_2O_2) and hypochlorous acid, effectively killing the engulfed microorganisms (8). Genetic mutations in NOX2 may lead to defective catalytic activity of the oxidase in X-linked inheritance, whereas mutations in other components of phagocyte NADPH oxidase may lead to autosomal recessive CGD (1, 2). A search of the human genome identified homologs of the gp91^{phox}-encoding genes and the establishment of the NADPH oxidases (NOX) family (9). Of the 7 NOX members, NOX2 is the first identified and most extensively studied catalytic subunit despite its name (10, 11), and a causal relationship between genetic deficiency of NOX2 and X-CGD is well established.

Essential for reactive oxygen species (EROS) is a protein identified in 2017 through a mouse screen for host genetic factors that confer susceptibility to attenuated *Salmonella typhimurium* infection (12). Thomas and coworkers found that an uncharacterized open reading frame bc017643 was highly conserved with the human ortholog C17ORF62 involved in the respiratory burst (12), that led the same group to associate mutations of this gene (*CYBC1*) with X-linked CGD with loss of NOX2 expression (13). Since 2018, several cases of this rare form of CGD have been reported (13–16). EROS, that contains

Author contributions: S.L. and R.D.Y. designed research; S.L., A.L., Y. Liu, F.W., Y.Z. and Y. Long performed research; A.L., T.W., Z.L. and R.R. contributed new reagents/analytic tools; S.L., A.L., Y. Liu and R.D.Y. analyzed data; S.L. and Y.Z. purified proteins; A.L. collected and processed cryo-EM data, built the structural model; F.W. and Z.L. collected cryo-EM data; R.D.Y. supervised research; and S.L., A.L., Y. Liu, and R.D.Y. wrote the paper.

The authors declare no competing interest.

This article is a PNAS Direct Submission.

[1]S.L. and A.L. contributed equally to this work.

[2]To whom correspondence may be addressed. Email: richardye@cuhk.edu.cn.

This article contains supporting information online at https://www.pnas.org/lookup/suppl/doi:10.1073/pnas.2320388121/-/DCSupplemental.

Published May 28, 2024.

187 amino acids, was predicted to be a membrane protein with two α-helices (12). It was subsequently confirmed that EROS associates closely with NOX2, in particular, the newly synthesized NOX2 polypeptide of 58 kDa in the endoplasmic reticulum (ER) (17). EROS binding of NOX2 protects the catalytic subunit from rapid degradation (17). Published work has shown that EROS binding precedes heme incorporation into and $p22^{phox}$ association with NOX2 (17). Based on these findings, EROS is defined as a molecular chaperone of NOX2 that is essential for its maturation and transport through the Golgi apparatus, where additional carbohydrate moieties on the N-linked high-mannose glycans are acquired. This function of EROS has been confirmed in genetically altered mice and in transfected cell lines (17).

Biochemical and cellular studies have shown that EROS directly binds NOX2, but the domains and amino acid residues involved in this interaction remain unidentified. Moreover, it is unclear whether EROS continues to bind NOX2 as it matures and moves to the plasma membrane, and whether this association has a functional impact on NOX2 activation. To address these questions, we characterized EROS in neutrophil-like HL-60 promyelocytic cells and found colocalization of EROS with mature NOX2. Using a mammalian expression system, we reconstituted a protein complex containing EROS, NOX2, and $p22^{phox}$. An analysis of samples collected from size-exclusion chromatography found both mature NOX2 and EROS in the same fraction. We then resolved the structure of the protein complex by single-particle cryogenic electron microscopy (cryo-EM). Our structural model identifies key interacting residues between the transmembrane (TM) helices of EROS and TM2 and TM6 of NOX2 that contribute to conformational alteration of these helices. There are extensive interactions between the C terminal Pleckstrin homology (PH) domain of EROS and the dehydrogenase (DH) domain of NOX2 that contains binding sites for flavin adenine dinucleotide (FAD) and NADPH. These findings indicate alteration of the electron transfer pathway due to EROS binding, suggesting that EROS stabilizes NOX2 in a protected conformation.

Results

EROS Binding to Mature NOX2. Recent studies have shown that EROS binds NOX2 in the ER, an event that occurs early in NOX2 biosynthesis (13, 17). In the ER, EROS serves as a molecular chaperone for NOX2 maturation and prevents degradation of newly synthesized 58 kDa polypeptide of NOX2 (17). However, it is unclear whether EROS remains associated with NOX2 after its maturation. We detected cell surface expression of EROS in differentiated neutrophil-like HL-60 cells (dHL-60) using a FITC-labeled anti-EROS. As shown in *SI Appendix*, Fig. S1, EROS (green fluorescence, 1B) was clearly visible against IgG-FITC control (1A) in dHL-60 cells. We used 7D5, an anti-NOX2 mAb (18) that recognizes fully glycosylated NOX2 (19), to stain dHL-60 together with a PE-labeled anti-mouse secondary antibody. NOX2 expression (red fluorescence) overlapped with EROS expression (green fluorescence) with the merged image showing yellow fluorescence (*SI Appendix*, Fig. S1*B*). To eliminate possible staining artifact and further confirm colocolization of EROS and NOX2, fusion proteins of EROS–mRuby2 (red fluorescence) and Clover-NOX2 (green fluorescence) were prepared and cotransfected into COS-7 cells. Colocalization of EROS and NOX2 was observed in COS-7 cells in a scattered pattern throughout the cells (*SI Appendix*, Fig. S1*C*). To determine whether EROS and NOX2 were expressed on the cell surface, intact dHL-60 cells were subject to flow cytometry using the same FITC-labeled anti-EROS and 7D5 plus PE-labeled anti-mouse secondary antibody. As shown in *SI Appendix*, Fig. S1*D*, about two-thirds of dHL-60 cells were stain positive with anti-NOX2 (*y* axis) and 30% of the cells were positive with EROS (*x* axis). In these cell populations, about 23% were double-positive after normalization against the IgG isotype controls. These findings demonstrate the ability of EROS to bind the fully glycosylated NOX2, but the majority of NOX2 is dissociated from EROS on the cell surface of the dHL-60 cells studied. In subsequent experiments, cell lysate was collected from Expi-HEK293F cells cotransfected with expression plasmids of EROS, NOX2, and FLAG-tagged $p22^{phox}$ for copurification of proteins. The eluent of cell lysate was affinity purified using anti-FLAG and incubated with the 7G5 Fab that recognizes an extracellular loop of mature NOX2 (20). Size-exclusion chromatography (SEC) was performed and two major peaks were obtained (*SI Appendix*, Fig. S2*A*). The collected peak fractions were resolved on SDS-PAGE (*SI Appendix*, Fig. S2*B*). The large peak fraction contained the mature NOX2 (approx. 91 kDa), 7G5 Fab (approx. 26 kDa), and EROS and $p22^{phox}$ (both running at approx. 22 kDa), indicating association of these proteins in a complex.

Overall Structure of the EROS–NOX2–$p22^{phox}$ Complex. The large peak fraction from SEC contained an EROS–NOX2–$p22^{phox}$ complex stabilized by the 7G5 Fab. This fraction was subject to single-particle analysis by cryo-EM (*SI Appendix*, Fig. S2 and S3), as detailed in *SI Appendix*, *Materials and Methods*. Electron density map of the complex (Fig. 1*A*) showed an overall resolution of 3.56 Å with 2 transmembrane (TM) helices of EROS, in addition to the 6 TM domains of NOX2 and 4 TM bundles of $p22^{phox}$ that were reported in recent publications (20, 21). An intracellular view of the complex (*Right* panel in Fig. 1*A*) found that EROS and $p22^{phox}$ are on opposite sides of NOX2 with a plane angle of 177°. With EROS included, the complex has a maximal base width of 85 Å, increasing from 60 Å in the absence of EROS (21).

A molecular model of EROS-NOX2-$p22^{phox}$ was built based on the cryo-EM electron density map. In this model (Fig. 1*B*), NOX2 contains two hemes (maroon) in between TM3 and TM5. There is also a streak of lipids (light blue) in the NOX2-$p22^{phox}$ interface. There are three carbohydrate moieties in the extracellular loops of NOX2 on asparagines N132, N149, and N240 (22). The EROS protein in this model shows 4 α-helices, of which H1 and H2 separate the PH domain of EROS and are connected by Loop 1 (L1). The two helices, about four to five turns each, are shorter than the TMs of NOX2 (seven to nine turns). The shortest helix (H3) has only three turns and is nearly perpendicular to the plane of H1 and H2. The H4 helix is located intracellularly and is only 24 amino acids away from the C-terminal end. Between H2 and H4 there are six β-strands, of which the two longest ones are connected by loop 2 (L2; Fig. 1 *C* and *D*). These structures constitute the majority of the PH domain that interacts with the cytoplasmic tail of NOX2 as detailed below.

The EROS–NOX2 Interface. An analysis of the complex structure identified extensive interactions between EROS and NOX2 (Fig. 2*A*). The EROS–NOX2 interface is composed of three parts. The first is in the transmembrane portion and is formed by the interactions between TM2, TM6 of NOX2 and H1, H2, and intracellular β-strands of EROS (Fig. 2*B*). This part includes multiple hydrophobic interactions and polar contacts including a hydrogen bond between Y51 (H2) of EROS and W270 (TM6) of NOX2. In addition, R22, N62, E115, and Q140 of EROS bind to the TM2 and loop B (LB) of NOX2 through polar interactions. These interactions allow EROS to wrap around TM2 and LB of NOX2 (Fig. 2*C*), thereby facilitating the insertion of EROS

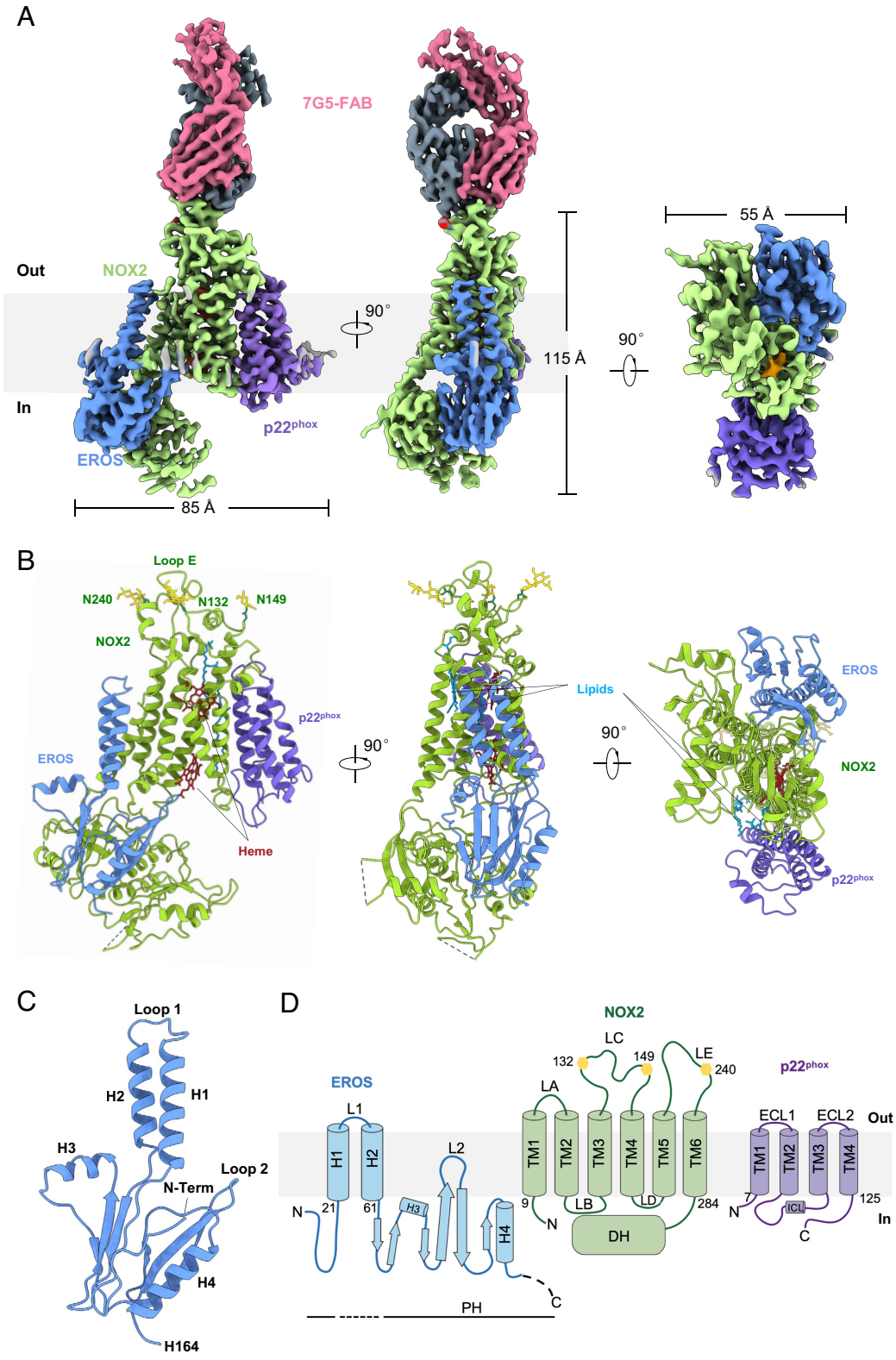

Fig. 1. Overall structure of the EROS–NOX2–p22^{phox}–7G5 complex. (*A*) Electron density map of the EROS–NOX2–p22^{phox}–7G5 complex. EROS (blue) and p22^{phox} (purple) are opposite to each other and both associated with NOX2 (green). For clarity, the 7G5–Fab dimers are colored differently in pink and gray. The *Left* panel shows a side view of the cryo-EM density map, and the middle panel depicts a 90° rotation to the left panel. The *Right* panel is a bottom view of the complex from an intracellular perspective. The inner heme (orange) is visible in this view. (*B*) 3-D reconstruction of the EROS–NOX2–p22^{phox} complex, showing NOX2 in green, EROS in blue and p22^{phox} in purple. The heme groups are marked in maroon. N-glycan moieties (yellow) at asparagines 132, 149, and 240 are shown on top of NOX2. A lipid streak (light blue) is visible in the *Middle* (horizontal 90° counter clock rotation) and *Right* (vertical 90° clockwise rotation) panels. (*C*) Cartoon representation of the EROS structure. There are four helices (H1 to H4) and six β strands, with the N terminus buried inside and the C terminal fragment (C165-S187) invisible due to insufficient electronic density. H1 (I21–Y40) and H2 (W47–Q61) are connected by loop 1; H3 (L85–F93) is nearly perpendicular to H1 and H2. The C terminal H4 (R147–L161) is tilted relative to plasma membrane. The two longest β-strands are antiparallel and connected by loop 2 (V117–G121). (*D*) Topological model of EROS (blue), NOX2 (green), and p22^{phox} (purple) in plasma membrane. The yellow hexagons indicate three glycosylation sites on NOX2. LA-LE corresponds to loop A to loop E. DH denotes the dehydrogenase domain of NOX2. PH (line at bottom) represents the Pleckstrin Homology domain separated by H1 and H2. L1 and L2 refer to loop 1 and loop 2. ECL and ICL stand for extracellular and intracellular loops, respectively.

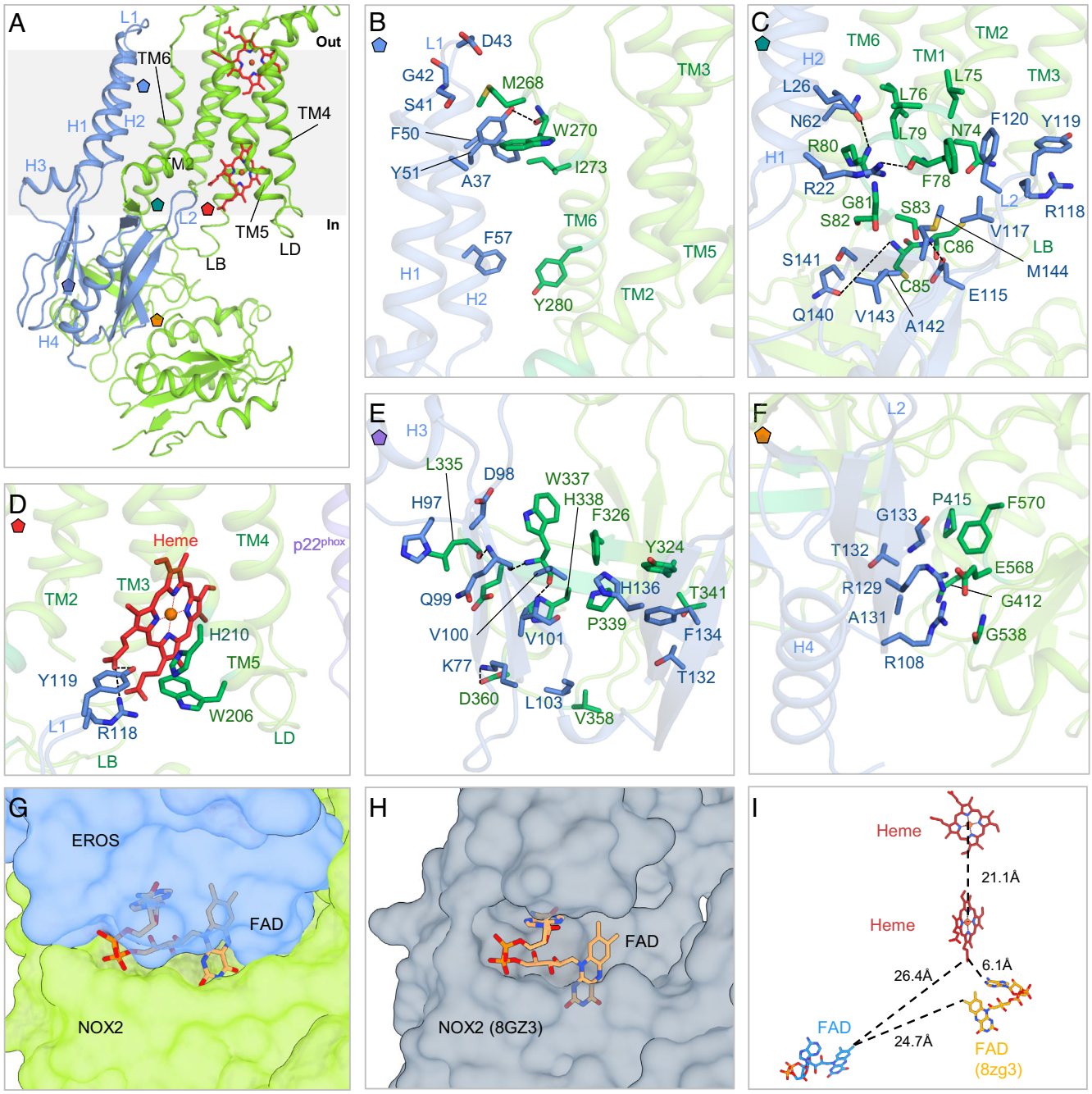

Fig. 2. The EROS–NOX2 interface. (*A*) Structural model of EROS (blue)–NOX2 (green), viewed parallel to the membrane. Membrane boundaries are shown in gray. Pentagons labels refer to zoomed views shown in the panel. (*B*) Interactions between H1 and H2 of EROS and TM6 of NOX2. The EROS residue Y51 is involved in hydrogen bonding with NOX2 residue W270. The residues of EROS and NOX2 are shown in blue and green sticks, respectively; the hydrogen bonds are represented by dark dash lines. (*C*) Interactions between H1 and H2 of EROS and TM2 and loop B of NOX2. EROS residues R22 and N62 form polar interaction with NOX2 residues F78 and R80, respectively. Two other EROS residues, E115 and Q140, form polar contacts with NOX2 residues C86 and C85 on Loop B, respectively. (*D*) Interaction of the inner heme (maroon) with R118/Y119 of EROS. Hydrophobic interactions between R118/Y119 of EROS and W206/H210 of NOX2 in TM5 are also shown. The main chain of L335/W337 of NOX2 form polar interactions with Q99 of EROS, and W337 main chain also has a polar contact with V101 of EROS. (*E*) A total of 20 amino acids, 10 each from EROS and NOX2, are involved in the EROS–NOX2 interface in the FAD-binding subdomain. (*F*) The EROS–NOX2 interface in the NADPH-binding domain of NOX2. Cartoon and surface representation of FAD binding to NOX2 (green) in the presence of EROS (blue in *G*) and in its absence (*H*, NOX2 is shown in gray). (*I*) Schematic representation of the electron transfer pathway showing the relative positions and distances between FAD and the two hemes in the absence (FAD in orange) and presence (FAD in blue) of EROS. The edge-to-edge distance between the inner heme and FAD in resting NOX2 (6.1 Å, 8GZ3) is shorter than that in EROS–NOX2 (26.4 Å). The ferric ions are shown as orange spheres.

loop 2 (R118, Y119) for interaction with the inner heme and TM5 (Fig. 2*D*). Consequently, the inner heme shifted its position downward by a few angstroms, and the center-to-center distance between the two hemes extended from 19.8Å without EROS (21) to 21.1Å in the presence of EROS (Fig. 2*I*).

The second part involves a subdomain where NOX2 binds to FAD, which is a part of the cytoplasmic dehydrogenase homology (DH) domain (6, 23). The importance of this domain in the initiation of transmembrane electron transfer is evidenced by more than 50 genetic mutations (*SI Appendix*, Fig. S4*A*) including 19 missense mutations in this region that contribute to CGD (23). In this subdomain (Fig. 2*E*), residues L335/W337 of NOX2 form polar interactions with Q99 of EROS, and W337 also has a polar contact with V101 of EROS. Furthermore, there are multiple

hydrophobic interactions between the β-strands of EROS and FAD-binding domain of NOX2. These hydrophobic interactions, combined with polar contacts, form a tight binding interface. Of note, H338Y, P339H, and T341K substitutions (*SI Appendix*, Fig. S4*B*) resulting from missense mutations of *CYBB* (encoding NOX2) are found in CGD patients and their influence on FAD binding has been proven in reconstituted PLB-985 cells (23). These observations suggest that the presence of EROS may interfere with FAD binding to the DH domain as shown in Fig. 2*G*, which is consistent with the absence of FAD in our solved cryo-EM structure. Moreover, when we fitted our model with that of the FAD-bound NOX2 (PDB ID: 8ZG3), three EROS amino acids (V101, L103, and F134) conflicted with FAD binding (Fig. 2*E*). These findings support the notion that EROS bind prevents FAD access to the DH subdomain, as schematically illustrated in Fig. 2 *G* and *H*. However, EROS binding is not expected to block $p67^{phox}$ access to NOX2, as this binding site (a.a. 369–383) (24, 25) does not participate in EROS interaction (*SI Appendix*, Fig. S4 *C* and *D*).

The third region is the DH subdomain that binds NADPH. In this region, the residues (G412/P415/G538/E568/F570 of NOX2) form tight hydrophobic interactions with EROS residues R108/R129/A131/T132/G133, respectively (Fig. 2*F*). Previous studies have shown that the affinity of resting NOX2 for NADPH is lower than that for FAD (26); in the presence of EROS, the ability of NOX2 to bind NADPH might be further compromised based on our structural analysis. Moreover, missense mutations causing the G412R, P415H, and E568K substitutions (*SI Appendix*, Fig. S4*B*) have been reported in CGD patients (5), indicating the importance of this subdomain of NOX2 in binding NADPH and possible interference by the bound EROS.

The EROS-Bound NOX2 Is in a Protected State. In the tight binding interface of EROS–NOX2, the presence of EROS induced conformational changes of NOX2 with an impact on its function. H1 of EROS is juxtaposed to TM2 of NOX2, and their interaction causes a 79° upward rotational shift of TM2 (a.a. 67–83) (Fig. 3 *A* and *C*) compared with the recently reported NOX2–$p22^{phox}$ structure (PDB ID: 8GZ3). H2 of EROS is closely associated with TM6 of NOX2, inducing a 48° clockwise turn of TM6 (a.a. 265–292) (Fig. 3 *B* and *D*). An extracellular view (Fig. 3*E*) and intracellular view (Fig. 3*F*) were provided, along with a movie showing these changes in motion (Movie S1) for better appreciation of these structural alterations in NOX2 induced by EROS binding.

Analysis of the structure of the EROS–NOX2–$p22^{phox}$ suggests that EROS association with the intracellular region of NOX2 interferes with FAD and NADPH access to the DH domain. The resulting changes may impact the electron transfer pathway of NOX2, thereby preventing spontaneous activation during its maturation and transport to plasma membrane. We examined the impact of activation signals on EROS–NOX2 association. NOX2 expression is induced in dHL-60 cells (Fig. 4*A*). Stimulation of dHL-60 with phorbol myristate acetate (PMA), an activator of NOX2, increased FAD association (Fig. 4*B*). To determine whether EROS association is dynamic with respect to NOX2 activation, a NanoLuc complementation assay (17, 27) was adopted to measure the dynamic changes in distance between the N-terminal end of EROS (fused with LgBiT) and C terminal end of NOX2 (fused with SmBiT). The expression plasmids containing these engineered EROS and NOX2 fusion constructs (schematically shown in Fig. 4*C* and detailed in *SI Appendix*, Materials and Methods) were cotransfected into COS-7 cells together with plasmids expressing the necessary cytosolic factors for reconstitution of active NOX2. Upon PMA stimulation, the changes in luminesce were measured to reflect the degree of association between EROS and NOX2. As shown in Fig. 4*D*, PMA induced a time-dependent dissociation of EROS from NOX2. Under the same stimulation conditions, PMA induced superoxide production in the reconstituted COS-7 cells ($COS^{91/22}$) that were significantly inhibited by overexpression of EROS (Fig. 4*E*). Together, these results suggest that activation signals may induce conformational changes in the complex, thereby increasing binding of FAD and production of superoxide in the tested model.

Discussion

In this study, we present a high-resolution cryo-EM structure of the EROS–NOX2–$p22^{phox}$ complex. The structure covers the entire EROS protein except the C terminal 23 amino acids, where the density is not well ordered. An analysis of the structure revealed that there is no direct interaction between EROS and $p22^{phox}$ since these two proteins are separated by NOX2, raising interesting possibilities for NOX2 protection as discussed below. EROS associates with the TM helices of NOX2 through H1 (interacting with TM2) and H2 (interacting with TM6), causing conformational changes in both TM helices. Of note, the cytoplasmic β-strands of EROS form extensive interactions with the cytoplasmic tail of NOX2 including the DH domain that harbors the FAD and NADPH binding sites. These interactions are expected to interfere with NOX2 binding of FAD and NADPH. Of note, the cryo-EM structure of the EROS–NOX2–$p22^{phox}$ complex does not contain FAD or NADPH, whereas the NOX2–$p22^{phox}$ complex (without EROS) solved in a recent study contains FAD (21). There is also a pocket-like structure on EROS that interacts with part of the TM2 and loop B of NOX2. This loop between TM2 and TM3 is very close to loop 2 of EROS such that a hydrogen bond is formed with the inner heme. Altogether, EROS binding of NOX2 induces structural changes that are expected to alter the electron transfer pathway by increasing the distance between the hemes, inducing a shift of the FAD binding site, and partially blocking the NADPH binding site in the DH domain. When this paper is under revision, Liu et al. published the structure of an active NOX2 (28). A comparison of the active and resting state structures showed that shortening the distance between critical points of the electron transfer pathway is a mechanism for NOX2 activation, which supports the notion that increasing the distance between the hemes in EROS-bound NOX2 impedes superoxide production.

The discovery of EROS as a critical component of host defense through NOX2 expression (12) is a major advancement in NOX2 biology and its deficiency becomes a new cause for CGD (13–15). Through a series of elegant experiments, Thomas and coworkers showed that EROS associates with the immature (58 kDa) NOX2 polypeptide in the ER and prevents its degradation (17). Although EROS is considered an ER resident protein, its primary sequence does not contain a typical ER-retention motif (29, 30). EROS associates with NOX2 before heme incorporation (17), whereas $p22^{phox}$ binds NOX2 after heme incorporation and addition of high-mannose N-glycans (19, 31). These observations indicate that NOX2 polypeptide first forms a heterodimer with EROS and then a heterotrimer with the addition of $p22^{phox}$. Both EROS and $p22^{phox}$ play important roles in NOX2 maturation from precursor (65 kDa) and in efficient transport of NOX2 to plasma membrane (17, 31). Our finding that EROS associates with mature NOX2 suggests that a portion of EROS–NOX2–$p22^{phox}$ remains in complex as they go through the Golgi apparatus where NOX2 acquires additional and complex N-glycans (19). Given the 1:1 stoichiometry of NOX2 and $p22^{phox}$ in the heterodimer (32) and the 1:1:1 stoichiometry of EROS:NOX2:$p22^{phox}$ in the solved structure,

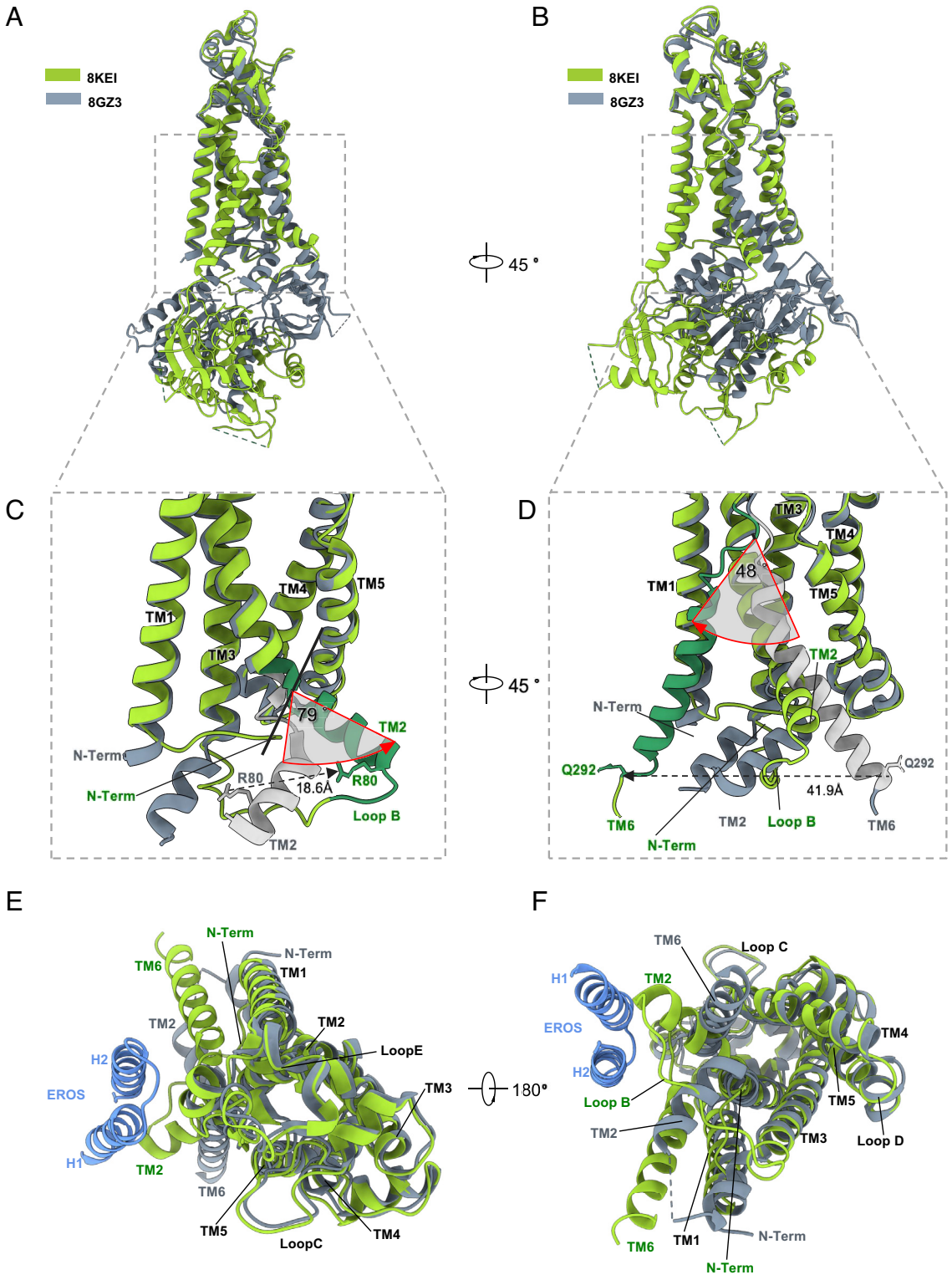

Fig. 3. Changes in NOX2 structure in the presence of EROS. (*A*) Superimposed 3-D structures of EROS–NOX2 from this study (8KEI, green, with EROS removed) with NOX2 in resting state (8GZ3, gray). (*B*) A 45° horizontal clockwise rotation of *A*. (*C*) Detailed view of boxed region in A showing a 79° upward bend (red arrow) of TM2 in the presence of EROS (removed for clarity) vs. its absence (silver). There is a 18.6 Å shift of R80, which is located at the bottom of TM2. (*D*) A 45° horizontal rotation of C showing a 48° backward rotation of a.a. 265–292 (dark green) of TM6 induced by EROS (removed). Compared with TM6 in the absence of EROS (8GZ3, silver), the bottom of TM6 represented by Q292 shifted by 41.9Å. (*E*) *Top* view (extracellular view, left) and (*F*) *Bottom* view (intracellular view, right) of the superimposed NOX2 structures in EROS-bound (green) and resting state (gray), with emphasis on the dislocated TM2 and TM6 of NOX2. EROS is marked in blue.

the interactions between these proteins are of special interest. It is notable that EROS and $p22^{phox}$ do not contact each other, suggesting that these two proteins have distinct functions in protecting NOX2 against proteolytic degradation as well as regulation of NOX2 activation.

NOX2 is the catalytic subunit of phagocyte NADPH oxidase that has all the structural features for one-electron reduction of molecular oxygen, including two nonidentical hemes between TM3 and TM5 and binding sites for the cofactor FAD and substrate NADPH (6, 7, 19, 26). While $p22^{phox}$ and EROS are not

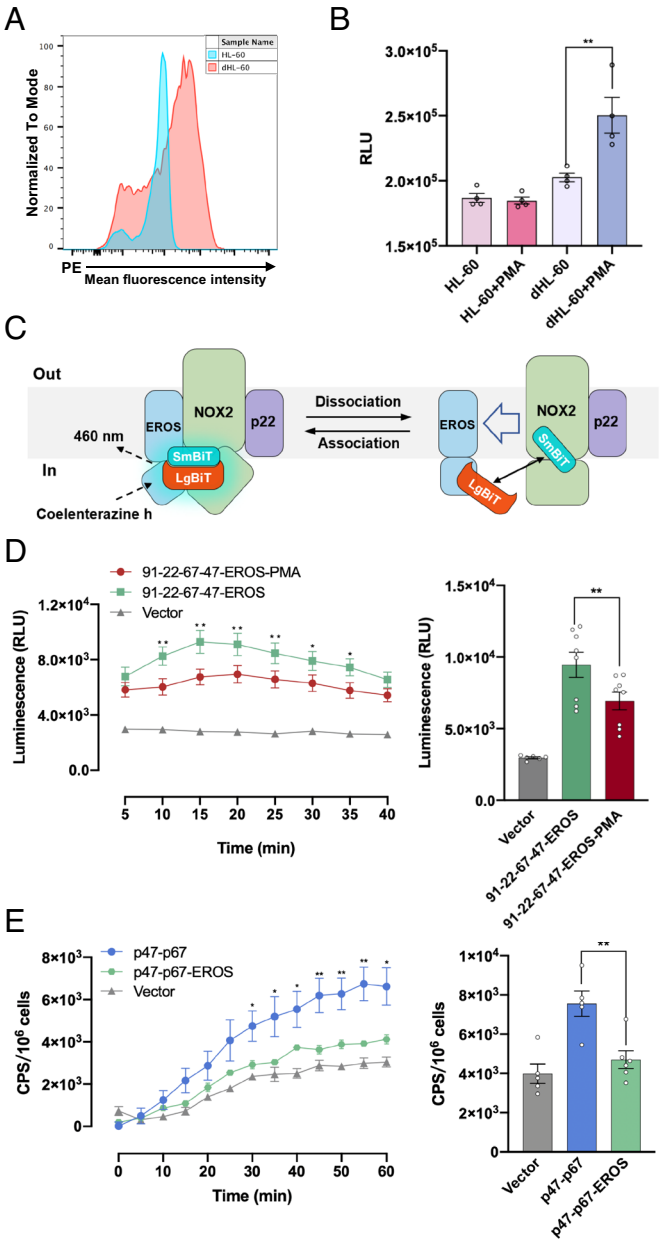

Fig. 4. The EROS-bound NOX2 in an inactive state. (*A*) Histogram of flow cytometric measurement of NOX2 expression in HL-60 (red) and dHL-60 (blue, 1.3% DMSO for 6 d). The 7D5 mAb (primary) and PE-conjugated anti-mouse mAb (secondary) were used. Relative expression level is shown in the *y* axis after normalization against maximal cell count. (*B*) FAD incorporation in the membrane fractions of HL-60 and dHL-60 without and with PMA (80 ng/mL) stimulation. $^{**}P < 0.01$. (*C*) Schematic representation of NanoLuc complementation assay. Engineered constructs (EROS–N-LgBiT, NOX2–C-SmBiT) were cotransfected into COS-7 cells together with the $p47^{phox}$ and $p67^{phox}$ expression plasmids. The changes in luminescence intensity were recorded, after addition of the substrate coelenterazine H (10 μM) and PMA (200 ng/mL), with a 5 min interval at 460 nm. Hypothetical dissociation of EROS from NOX2 is indicated by an arrowhead, and data collected are shown in (*D*). (*E*) Superoxide production in reconstituted COS-7 cells ($COS^{91/22}$) cotransfected with expression plasmids of $p47^{phox}$, $p67^{phox}$, with or without an EROS expressing plasmid. The PMA-induced superoxide production was measured in real time for 60 min using isoluminol, and data were quantified and presented in the *Right* panel. Data shown are mean ± SEM based on multiple independent experiments. $^{*}P < 0.05$, $^{***}P < 0.001$.

directly involved in the transfer of electrons to molecular oxygen (6), they are necessary for NOX2 maturation. In addition to providing a docking site for $p47^{phox}$ membrane translocation (33, 34), $p22^{phox}$ has been known to stabilize the newly synthesized and heme-incorporated NOX2. Both EROS and $p22^{phox}$ associate with NOX2 with their TM helices. There are, however, significant differences between EROS and $p22^{phox}$ in their interaction with the C terminal cytoplasmic region of NOX2. While recently published NOX2 structural models (20, 21) and the present study do not show any interaction between the cytoplasmic domains of NOX2 and $p22^{phox}$, our work provides direct evidence for a close interaction between EROS and NOX2 in their C terminal cytoplasmic fragments including formation of multiple hydrogen bonds involving the DH domain of NOX2 that contains binding sites for FAD and NADPH. Previous studies have shown that missense mutations of amino acid residues in this region can cause CGD through the disruption of the electron transfer pathway (23). It is therefore hypothesized that the EROS-bound NOX2 is protected against proteolytic degradation as well as binding of FAD and NADPH that initiates electron transfer for superoxide production. This "protected state" of NOX2 is conceptually different from the previously proposed "resting state," which emphasizes NOX2 conformation before assembly of the active complex. Instead, NOX2 in the protected state is held incapable of initiating electron transfer because of its binding to EROS. This may be necessary to prevent inadvertent production of superoxide and ensure proper maturation and membrane transport of NOX2, as a previously published study showed that the purified and relipidated flavocytochrome b558 was able to generate superoxide in a FAD-and NADPH-dependent but cytosolic factor-independent manner (35). Published study has also indicated that FAD binding to NOX2 may be a critical regulatory step for superoxide production (36). Given the high affinity of FAD for the DH domain and the abundance of NADPH in the cytosolic compartment, spontaneous activation of NOX2 must be properly controlled and EROS binding may provide this mechanism.

The NOX2 activation mechanism is the most complicated among all NOX family members with respect to the proteins associated with the catalytic subunit. These protein factors interact with NOX2 in different ways. While $p67^{phox}$ binds directly to NOX2 (24, 25), $p47^{phox}$ interacts with $p22^{phox}$ and may influence NOX2 indirectly (37). Some of these factors are not associated with the resting-state NOX2 (e.g., $p67^{phox}$ and Rac) (11, 38, 39), whereas $p22^{phox}$ remains associated even after membrane protein purification. As described in *SI Appendix, Materials and Methods*, the EROS–NOX2–$p22^{phox}$ heterotrimer is preserved only when a special blend of detergents is used. EROS does not appear in complex with flavocytochrome b558 when detergents such as octyl glucoside are applied in membrane purification, which may explain why EROS escaped from attention until a genetic study identified its association with CGD (12). Our structural analysis suggests that EROS must dissociate from NOX2 to allow electron transfer and superoxide production, and there is an association between increased FAD binding and induced superoxide production. Our flow cytometry analysis of dHL-60 cells indicates that the majority of EROS-bound flavocytochrome b558 arrives to cell surface without the bound EROS, leaving one to speculate that EROS dissociation from NOX2–$p22^{phox}$ occurs en route from Golgi to plasma membrane. The mechanisms for EROS dissociation have not been elucidated, and it remains interesting to determine whether flavocytochrome b558 destined for intracellular granules is associated with EROS. For the small fraction (≤23%) of EROS-associated NOX2–$p22^{phox}$ on cell surface, their fate may be influenced by activation signals such as PMA. It is therefore important to know whether EROS association and dissociation with flavocytochrome b558 is a dynamic process subject to regulation by signaling pathways. This work will be best accomplished in EROS-deficient myeloid cell lines, such as genetically altered PLB-985, to overcome limitations of the present study including

using a polyclonal anti-EROS antibody in a nonmyeloid cellular environment. If the dynamic regulation can be proven, then EROS may serve to regulate the pool size of NOX2-p22^{phox} available for activation in addition to its original function as a molecular chaperone.

Materials and Methods

Detailed protocols are provided in *SI Appendix, Materials and Methods* section.

Plasmid Vector Construction. Wildtype human NOX2 and N-terminal FLAG tag-p22^{phox} were cloned into the pMlink vector (40). The DNA coding sequences for wildtype human EROS, 7G5 Fab heavy chain and light chain were then cloned into other pMlink vectors for coexpression of the relevant proteins. N-clover–NOX2 and C-mRuby2–EROS were cloned into the pcDNA3.1 expression plasmid (Invitrogen). For NanoBiT-based assay, the LgBiT coding sequence was fused to the N terminus of EROS to generate pcDNA3.1–N-LgBiT–EROS. The SmBiT coding sequence was fused to the C terminus of NOX2 coding sequence to generate pCDNA3.1–NOX2–C-SmBit. The cDNAs of human p47^{phox} and p67^{phox} were cloned into pcDNA 3.1. For details, please refer to *SI Appendix, Materials and Methods*.

7G5 Fab Purification. 7G5 Fab (20) were expressed in transiently transfected Expi-293F cells (Thermo Fisher Scientific) and purified by affinity chromatography using protein A/G agrose (Beyotime). The elution was collected and incubated with EROS–NOX2–p22^{phox} preparation for complex formation.

Complex Purification. Expi–293F cells were cultured in FreeStyle 293 medium (Union Biotech) and cotransfected with pMlink-N-FLAG–p22^{phox}–NOX2 and pMlink-EROS. The transfected cells were cultured for 48 h and collected. The cells were lysed by lysis buffer and purified by anti-FLAG affinity resin. The 7G5 fab was incubated with EROS–NOX2–p22^{phox} complex before size-exclusion chromatography (SEC). These experiments are described in detail in *SI Appendix, Materials and Methods*.

Cryo-EM Grid Preparation and Data Collection. For cryo-EM grid preparation, purified complex was deposited onto a glow-discharged holey grid. It was then plunge-frozen in liquid ethane using the Vitrobot Mark IV (Thermo Fischer Scientific). Cryo-EM images were obtained on a Titan Krios C3i cryo-TEM (Thermo Fisher Scientific) operating at 300 kV, using a K3 Summit detector (Gatan) with a pixel size of 0.85 Å. Acquisition parameters are detailed in *SI Appendix, Materials and Methods*.

Cryo-EM Image Processing and Map Construction. The cryoSPARC v3.3.1 software (Structura Biotechnology) was utilized to perform single particle analysis of the EROS–NOX2–p22^{phox}–7G5 complex After multiple rounds of refinement, a final set of 131,926 particles underwent nonuniform refinement and local refinement, resulting in a map with an overall resolution of 3.56 Å at a Fourier shell correlation of 0.143.

Model Building and Refinement. The initial model used for rebuilding and refinement against the electron microscopy density map was the model of the resting-state NOX2 (PDB: 8GZ3). The electron microscopy density map was docked with the model using UCSF Chimera-1.14, followed by iterative manual adjustment and rebuilding in COOT-0.9.8. The models were further refined and validated using the Phenix-1.20 programs. Structural figures were generated using UCSF Chimera-1.14, ChimeraX-1.27, and PyMOL-2.5. The data collection and structure refinement statistics are shown in *SI Appendix*, Table S1 and *Materials and Methods*.

Flow Cytometry Analysis. HL-60 cells differentiated with 1.3% DMSO for 6 d (dHL-60) were collected and harvested. The cells were stained with an anti-EROS FITC-conjugated antibody (CSB-PA859832LC01HU; CUSABIO Technology) or an anti-gp91^{phox} 7D5 antibody (D162-3; Medical & Biological Laboratories) with a fluorescent secondary antibody, or both anti-EROS FITC and anti-gp91^{phox} 7D5. The goat anti-mouse PE secondary antibody (12-4010-82; Thermo Fisher Scientific) was used. The cells were analyzed using flow cytometry on a CytoFLEX S flow cytometer (Beckman Coulter). This experiment is described in detail in *SI Appendix, Materials and Methods*.

Fluorescent Confocal Microscopy. For confocal microscopy, dHL-60 cells were fixed with 4% paraformaldehyde. The cells were incubated with anti-EROS–FITC and anti-gp91^{phox} 7D5 antibody overnight at 4 °C and then incubated with goat anti-mouse PE secondary antibody for 1 h. After removing the secondary antibody solution, the cells were washed with PBS and then incubated with DAPI for 5 min. Finally, a sealer containing an antifluorescence quencher was added to the slide.

COS-7 cells were cultured for 12 h on glass coverslips and then cotransfected with pcDNA3.1–NOX2–N-Clover and EROS–C-mRuby2 using Lipofectamine 3000 (Thermo Fisher Scientific) for 24 h at 37 °C. The coverslips were then mounted on glass slides and imaged using a confocal microscope (LEICA TCS SP8, Leica Microsystems). These experiments are described in detail in *SI Appendix, Materials and Methods*.

Superoxide Production Assay. COS$^{91/22}$ was prepared using the original protocol of Dinauer and coworkers (41) except that the p22^{phox} cDNA was expressed in pcDNA3.1-neuromycin vector (Thermo Fisher Scientific). Superoxide production in COS$^{91/22}$ cells was assessed using an isoluminol-enhanced chemiluminescence (ECL) assay in 6 mm wells of 96-well, flat-bottomed white tissue culture plates. For details, please refer to *SI Appendix, Materials and Methods*.

Detection of FAD Binding to NOX2. The membrane fractions of HL-60 and dHL-60 were prepared as previous study (23). The emission of FAD was measured at 535 nm after excitation at 450 nm using an Envision multimode plate reader (Perkin Elmer).

NanoBiT Based Assay. COS-7 cells were seeded and cotransfected with pcDNA3.1–N-LgBiT–EROS, pcDNA3.1–NOX2–C-SmBit, pcDNA3.1–p47^{phox,} and pcDNA3.1–p67^{phox} or empty vector using Lipofectamine 3000 for 24 h at 37 °C. The cells were harvested and then plated onto white 96-well plates. The transfected cells were stimulated with either PMA or buffer control. Next, coelenterazine H (Yeasen Biotechnology) was added to the plates. luminescence was measured on the plate using an Envision multimode plate reader for 35 min. This experiment is described in detail in *SI Appendix, Materials and Methods*.

Statistical Analysis. Prism software (ver. 8.0, GraphPad) was used for statistical analysis of data. For statistical comparison, one-way ANOVA was used. A P value of <0.05 was considered statistically significant.

Data, Materials, and Software Availability. The atomic coordinates for the model of EROS–NOX2–p22^{phox}–7G5 Fab complex have been deposited to the Protein Data Bank (PDB) under the accession code 8KEI (42). All other data are included in the manuscript and/or supporting information.

ACKNOWLEDGMENTS. We thank the High-Performance Computing Platform at The Chinese University of Hong Kong, Shenzhen for computational work. This study was supported in part by grants from the National Key R&D Program of China (Grant 2019YFA0906003); the Science, Technology and Innovation Commission of Shenzhen Municipality Grant GXWD20201231105722002-20200831175432002 (to R.D.Y.); Shenzhen Fundamental Research Program (No. SGDX20210823103804030); National Natural Science Foundation of China Grant 32070950 (to R.D.Y.); China Postdoctoral Science Foundation 2022M713049 (to A.L.) and Shenzhen Science and Technology Program Grant No. RCBS20221008093330067 (to A.L.); The Kobilka Institute of Innovative Drug Discovery at The Chinese University of Hong Kong, Shenzhen (Z.L., R.R., and R.D.Y.); and the Ganghong Young Scholar Development Fund (S.L., Y.Z., and R.D.Y.).

Author affiliations: [a]Kobilka Institute of Innovative Drug Discovery, School of Medicine, The Chinese University of Hong Kong, Shenzhen, Guangdong 518172, China; [b]Dongguan Songshan Lake Central Hospital, Dongguan Third People's Hospital, Dongguan, Guangdong 523326, China; [c]Institute of Infectious Diseases, Shenzhen Bay Laboratory, Guangming District, Shenzhen 518132, China; [d]Key Laboratory of Computational Chemistry and Drug Design, Peking University Shenzhen Graduate School, Nanshan District, Shenzhen 518055, China; [e]Shanghai Key Laboratory of Metabolic Remodeling and Health, Institute of Metabolism and Integrative Biology, Fudan University, Shanghai 200438, China; and [f]The Chinese University of Hong Kong, Shenzhen Futian Biomedical Innovation R&D Center, Shenzhen, Guangdong 518000, China

1. M. C. Dinauer, Chronic granulomatous disease and other disorders of phagocyte function. *Hematology Am. Soc. Hematol. Educ. Program* 89–95 (2005), 10.1182/asheducation-2005.1.89.
2. S. M. Holland, Chronic granulomatous disease. *Hematol. Oncol. Clin. North Am.* **27**, 89–99, viii (2013).
3. A. W. Segal, A. Abo, The biochemical basis of the NADPH oxidase of phagocytes. *Trends Biochem. Sci.* **18**, 43–47 (1993).
4. B. M. Babior, NADPH oxidase. *Curr. Opin. Immunol.* **16**, 42–47 (2004).
5. D. Roos *et al.*, Hematologically important mutations: X-linked chronic granulomatous disease (fourth update). *Blood Cells Mol. Dis.* **90**, 102587 (2021).
6. A. Vermot, I. Petit-Hartlein, S. M. E. Smith, F. Fieschi, NADPH Oxidases (NOX): An overview from discovery, molecular mechanisms to physiology and pathology. *Antioxidants (Basel)* **10**, 890 (2021).
7. A. W. Segal, O. T. Jones, Novel cytochrome b system in phagocytic vacuoles of human granulocytes. *Nature* **276**, 515–517 (1978).
8. W. M. Nauseef, Assembly of the phagocyte NADPH oxidase. *Histochem. Cell Biol.* **122**, 277–291 (2004).
9. J. D. Lambeth, G. Cheng, R. S. Arnold, W. A. Edens, Novel homologs of gp91phox. *Trends Biochem. Sci.* **25**, 459–461 (2000).
10. K. Bedard, K. H. Krause, The NOX family of ROS-generating NADPH oxidases: Physiology and pathophysiology. *Physiol. Rev.* **87**, 245–313 (2007).
11. E. Pick, "Paradigm shifts in the history of Nox2 and its regulators: An appreciative critique" in *NADPH Oxidases Revisited: From Function to Structure* (2023), pp. 3–63, 10.1007/978-3-031-23752-2_1. Springer.
12. D. C. Thomas *et al.*, Eros is a novel transmembrane protein that controls the phagocyte respiratory burst and is essential for innate immunity. *J. Exp. Med.* **214**, 1111–1128 (2017).
13. D. C. Thomas *et al.*, EROS/CYBC1 mutations: Decreased NADPH oxidase function and chronic granulomatous disease. *J. Allergy Clin. Immunol.* **143**, 782–785 e781 (2019).
14. G. A. Arnadottir *et al.*, A homozygous loss-of-function mutation leading to CYBC1 deficiency causes chronic granulomatous disease. *Nat. Commun.* **9**, 4447 (2018).
15. M. Chiriaco *et al.*, Characterization of AR-CGD female patient with a novel homozygous deletion in CYBC1 gene presenting with unusual clinical phenotype. *Clin. Immunol.* **251**, 109316 (2023).
16. P. M. Mortimer *et al.*, A novel mutation in EROS (CYBC1) causes chronic granulomatous disease. *Clin. Immunol.* **255**, 109761 (2023).
17. L. O. Randzavola *et al.*, EROS is a selective chaperone regulating the phagocyte NADPH oxidase and purinergic signalling. *Elife* **11,** e76387 (2022).
18. A. Yamauchi *et al.*, Location of the epitope for 7D5, a monoclonal antibody raised against human flavocytochrome b558, to the extracellular peptide portion of primate gp91phox. *Microbiol. Immunol.* **45**, 249–257 (2001).
19. L. Yu *et al.*, Biosynthesis of flavocytochrome b558. gp91(phox) is synthesized as a 65-kDa precursor (p65) in the endoplasmic reticulum. *J. Biol. Chem.* **274**, 4364–4369 (1999).
20. S. Noreng *et al.*, Structure of the core human NADPH oxidase NOX2. *Nat. Commun.* **13**, 6079 (2022).
21. R. Liu *et al.*, Structure of human phagocyte NADPH oxidase in the resting state. *Elife* **11**, e83743 (2022).
22. T. M. Wallach, A. W. Segal, Analysis of glycosylation sites on gp91phox, the flavocytochrome of the NADPH oxidase, by site-directed mutagenesis and translation in vitro. *Biochem. J.* **321**, 583–585 (1997).
23. F. Debeurme *et al.*, Regulation of NADPH oxidase activity in phagocytes: Relationship between FAD/NADPH binding and oxidase complex assembly. *J. Biol. Chem.* **285**, 33197–33208 (2010).
24. T. Fradin, E. Bechor, Y. Berdichevsky, I. Dahan, E. Pick, Binding of p67(phox) to Nox2 is stabilized by disulfide bonds between cysteines in the (369) Cys-Gly-Cys(371) triad in Nox2 and in p67(phox). *J. Leukoc Biol.* **104**, 1023–1039 (2018).
25. E. Bechor *et al.*, p67(phox) binds to a newly identified site in Nox2 following the disengagement of an intramolecular bond-Canaan sighted? *J. Leukoc. Biol.* **107**, 509–528 (2020).
26. A. R. Cross, A. W. Segal, The NADPH oxidase of professional phagocytes–prototype of the NOX electron transport chain systems. *Biochim. Biophys. Acta* **1657**, 1–22 (2004).
27. A. S. Dixon *et al.*, Nanoluc complementation reporter optimized for accurate measurement of protein interactions in cells. *ACS Chem. Biol.* **11**, 400–408 (2016).
28. X. Liu, Y. Shi, R. Liu, K. Song, L. Chen, Structure of human phagocyte NADPH oxidase in the activated state. *Nature* **627**, 189–195 (2024).
29. H. R. Pelham, Evidence that luminal ER proteins are sorted from secreted proteins in a post-ER compartment. *EMBO J.* **7**, 913–918 (1988).
30. M. R. Jackson, T. Nilsson, P. A. Peterson, Identification of a consensus motif for retention of transmembrane proteins in the endoplasmic reticulum. *EMBO J.* **9**, 3153–3162 (1990).
31. L. Yu, L. Zhen, M. C. Dinauer, Biosynthesis of the phagocyte NADPH oxidase cytochrome b558. Role of heme incorporation and heterodimer formation in maturation and stability of gp91phox and p22phox subunits. *J. Biol. Chem.* **272**, 27288–27294 (1997).
32. J. Huang, N. D. Hitt, M. E. Kleinberg, Stoichiometry of p22-phox and gp91-phox in phagocyte cytochrome b558. *Biochemistry* **34**, 16753–16757 (1995).
33. P. G. Heyworth *et al.*, Neutrophil nicotinamide adenine dinucleotide phosphate oxidase assembly. Translocation of p47-phox and p67-phox requires interaction between p47-phox and cytochrome b558. *J. Clin. Invest.* **87**, 352–356 (1991).
34. J. H. Leusen *et al.*, 156Pro->Gln substitution in the light chain of cytochrome b558 of the human NADPH oxidase (p22-phox) leads to defective translocation of the cytosolic proteins p47-phox and p67-phox. *J. Exp. Med.* **180**, 2329–2334 (1994).
35. V. Koshkin, E. Pick, Generation of superoxide by purified and relipidated cytochrome b559 in the absence of cytosolic activators. *FEBS Lett.* **327**, 57–62 (1993).
36. S. Hashida *et al.*, Binding of FAD to cytochrome b558 is facilitated during activation of the phagocyte NADPH oxidase, leading to superoxide production. *J. Biol. Chem.* **279**, 26378–26386 (2004).
37. J. El-Benna, P. M. Dang, M. A. Gougerot-Pocidalo, J. C. Marie, F. Braut-Boucher, p47phox, the phagocyte NADPH oxidase/NOX2 organizer: Structure, phosphorylation and implication in diseases. *Exp. Mol. Med.* **41**, 217–225 (2009).
38. A. Abo *et al.*, Activation of the NADPH oxidase involves the small GTP-binding protein p21rac1. *Nature* **353**, 668–670 (1991).
39. U. G. Knaus, P. G. Heyworth, T. Evans, J. T. Curnutte, G. M. Bokoch, Regulation of phagocyte oxygen radical production by the GTP-binding protein Rac 2. *Science* **254**, 1512–1515 (1991).
40. P. Lu *et al.*, Three-dimensional structure of human gamma-secretase. *Nature* **512**, 166–170 (2014).
41. M. O. Price *et al.*, Creation of a genetic system for analysis of the phagocyte respiratory burst: High-level reconstitution of the NADPH oxidase in a nonhematopoietic system. *Blood* **99**, 2653–2661 (2002).
42. S. Y. Liang, A. J. Liu, Y. Z. Liu, Cryo-EM structure of NADPH oxidase 2 in complex with p22phox and EROS. Protein Data Bank. https://www.rcsb.org/structure/8KEI. Deposited 11 August 2023.